Research Paper

2D Numerical Analysis of an H-Darrieus Hydrokinetic Turbine with Passive Improvement Mechanisms

Angie Judith GUEVARA-MUÑOZ[1)*], Diego Andrés HINCAPIE-ZULUAGA[1)],
Miguel Ángel RODRÍGUEZ-CABAL[1)], Jorge Andrés SIERRA-DEL-RIO[2)],
Ramón Fernando COLMENARES-QUINTERO[3)], Edwar TORRES-LOPEZ[4)]

[1)] *Department of Mechatronic Engineering, Research Group – MATyER*
Instituto Tecnológico Metropolitano
Medellín, Colombia

[2)] *Department of Mechanical Engineering, Research Group – GIIAM*
Institución Universitaria Pascual Bravo
Medellín, Colombia

[3)] *Faculty of Engineering, Universidad Cooperativa de Colombia*
Medellín, Colombia

[4)] *Department of Mechanical Engineering, Research Group – GEA*
Universidad de Antioquia
Medellín, Colombia

*Corresponding Author e-mail: angieguevara220191@correo.itm.edu.co

H-Darrieus hydrokinetic turbines are an alternative for small hydroelectric plants. These turbines are considered to have a low environmental impact as they do not require reservoirs. However, they have limited self-starting capacity, which limits their use. Nevertheless, the configuration of passive mechanisms in the H-Darrieus turbines affects their performance, as they tend to increase the flow velocity. This study is part of a project with the aim to design and build a turbine to generate energy in the Colombian river scenario in non-interconnected zones. The objective of this study is to analyze the performance through numerical simulations of four H-Darrieus rotors to be configured with passive improvement mechanisms. The study was conducted using ANSYS® Fluent software, employing transient, two-dimensional models under constant operating conditions. Overlapping meshes were used for the stationary and rotating domain configuration. The results show that increased solidity leads to decreased tip speed ranges and increased maximum rotor power. Improvement in the self-starting capability was found with passive mechanisms employing a diffuser geometry. Among the tested configurations, the rotor configured with a Venturi-shaped mechanism achieved a remarkable 660% improvement in the power coefficient compared to configurations without such mechanisms.

Keywords: renewable energy; H-Darrieus rotor; hydrokinetics; diffusers; computational fluids dynamics (CFD); external accessories.

1. Introduction

Improving renewable energy production systems is becoming increasingly important to meet global electricity demand. Currently, hydropower is the largest renewable energy source in the world, satisfying about 60% of all renewable energy globally [1]. Within this category of electrical installations are the small hydroelectric power plants (SHPPs), which are environmentally friendly sources of energy [2]. They require less engineering work and cost than the ones used for large power plants, making them ideal for rural electrification projects. Among the turbines used in SHPPs are hydrokinetic turbines that operate on the same operating principle as wind turbines [3, 4], but they harness the natural water currents to generate electrical energy. They are considered a viable option with low environmental impact [5] because they operate under zero head conditions. However, in countries such as Colombia, which possess great hydrological potential and have enormous needs in non-interconnected zones (ZNI), limited research and development of pilot projects using hydrokinetic technology have been reported [6].

One of the most common hydrokinetic turbines is the H-Darrieus turbine (HDT), which can be considered a viable option for hydrogenation [7, 8], because it can operate in rivers with varying ranges of velocities [9]. The blade geometry of an HDT is a critical characteristic greatly influencing the turbine's performance, due to the pressure forces that develop when it is subjected to incident flow. The lift forces on each blade contribute to the positive rotor torque, which is then transferred to the generator through the main shaft and other drive train components. Additionally, the number of blades is a fundamental parameter because it is directly related to solidity [10], and it has a big impact on the overall dynamic behavior of HDTs [11]. While two blades offer the highest efficiency, they also result in a higher negative torque coefficient [12–14]. This is why it is better to implement three blades, as it offers greater cyclic stability [15]. Solidity is a fundamental parameter that determines the geometry of HDTs and considerably influences their behavior [16]. For example, turbines with low solidity have better self-starting capacity [17]. Also, the point of maximum efficiency in the power coefficient (C_p) vs. tip speed ratio (TSR) curve of an HDT is decreased by increasing solidity having an impact on the operating range [18, 19]. Despite all the geometric parameters that have been evaluated to improve the efficiency of HDT, its self-starting capacity tends to be low. For this very reason, external assistance is needed to improve its performance. Therefore, several authors have studied the HDT configurations with external accessories, such as plates, nozzles, blades, diffusers, and area reductions in the channels to increase efficiency and reduce negative torque.

For example, Gosselin *et al.* determined that blade arrangement with plates at the end minimizes efficiency losses [20]. Additionally, Kumar *et al.* [21] studied a turbine with a double rotor and determined that this configuration offers improved self-starting, providing an initial torque advantage, but lowering the efficiency concerning the TSR and increased manufacturing and maintenance costs due to the additional rotor. At the same time, Shimokawa *et al.* [22] configured an H-Darrieus hydrokinetic turbine with an inlet nozzle of varying t depths depending on the flow. In addition, they determined that this implantation increased efficiency, although this depended on the flow level. In the same way, Hashem *et al.* [23] numerically evaluated 24 profiles and one HDT in configuration with different channel geometries. The S1046 profile exhibited a better performance, and the channels increased the power factor compared to 2D models without wind-lens. Similarly, Tunio *et al.* [24] configured an H-Darrieus hydrokinetic turbine in a duct with area reduction, which increased the power output by 112% for the non-duct configuration.

In addition, Patel *et al.* [25] conducted an experimental study with an H-Darrieus hydrokinetic turbine configured with a blocking plate, and it was concluded that the plate configuration directly impacts the performance. On the other hand, Janon [26] developed a three-dimensional numerical study using MATLAB and Visual Basic for an H-Darrieus hydrokinetic turbine with two rotors of NACA 0018 type profile arranged in series that have a gear mechanism. The study concluded that the configuration with four blades on each rotor at an offset angle of 45° yielded the best results. Based on the literature, it is evident that the use of passive mechanisms such as external accessories in the H-Darrieus hydrokinetic turbines increases efficiency. Likewise, it is necessary to evaluate different TSRs to find the maximum efficiency point.

For the reasons mentioned above, the objective of this study is to evaluate and numerically compare the impact of external accessories on the performance of four H-Darrieus hydrokinetic turbines with symmetrical profile type NACA 0018. The mentioned accessories consist of a blocking plate and three area reduction ducts with different geometries. Each case was configured with solidities of 1.0, 1.35, and 1.79. The numerical study was developed via Fluent simulation. The remainder of the study is divided in three parts. The first section describes the operational principles of the turbine and the research procedure. In the second section, the results of the torque coefficient and power coefficient of the turbines are analyzed and discussed. The last section presents the conclusions of the research.

2. Methodology

To study the hydrodynamic behavior of HDTs using CFD techniques, it is necessary to consider the mathematical expressions that describe the behavior of

these turbines. Once the most important parameters were established, a CFD simulation was performed using ANSYS® 2022R1. The mathematical model that describes the turbine design is presented below.

2.1. Operating principles

As the design of H-Darrieus hydrokinetic turbines is analogous to that of wind turbines, the available energy P_w in the water is estimated using Eq. (2.1):

$$(2.1) \qquad P_w = \frac{1}{2}\rho A U^3,$$

where ρ is the density, A is the projected area of the rotor, and U is the water velocity. The turbines do not have the capacity to extract all the available energy from the water. So, it is necessary to consider the power coefficient C_p to estimate the fraction of power that is extracted by the axis in an interval of a water stream passing through the cross-section A of the rotor [27]

$$(2.2) \qquad P_T = 0.5\rho A U^3 C_p.$$

Likewise, P_T is the output power of the H-Darrieus turbine that can be calculated using the equation:

$$(2.3) \qquad P_T = T\omega,$$

where T is the turbine shaft's torque and ω is the angular velocity. On the other hand, if we isolate C_p from Eq. (2.2), we obtain the power coefficient:

$$(2.4) \qquad C_p = \frac{P_T}{P_w}.$$

Usually, the most important parameters in HDT investigations are the power coefficient C_p and the torque coefficient C_t. These coefficients establish the relationship between the mechanical power output P_T and the torque of force T on the turbine shaft:

$$(2.5) \qquad C_p = \frac{P_T}{\frac{1}{2}\rho A U^3},$$

$$(2.6) \qquad C_t = \frac{T}{\frac{1}{2}\rho A U^2}.$$

Additionally, the rotor solidity σ is a fundamental parameter for defining the vertical axis turbine geometry because this parameter compares the number of blades N and their dimensions (chord length c) with respect to the turbine's rotation radius R, and this can be calculated as follows:

$$(2.7) \qquad \sigma = \frac{Nc}{R}.$$

2.2. Turbine design

Five simplified 2D models were designed in the SpaceClaim module of ANSYS® 2022, where each model has a rotor with three blades and one background grid. The blades employ a NACA 0018 profile with solidities of 1.0, 1.35, and 1.79. The rotor is represented by a circumference, and four background grids were designed to represent the water channel with passive mechanisms. In addition, a turbine without mechanisms (the baseline case) was designed. In this way, it is possible to compare the variety of the torque and power coefficient in cases with mechanisms with respect to the baseline case. The dimensions of the water channel are shown in Fig. 1a, while Fig. 1b shows the design parameters of the rotor and the passive mechanisms.
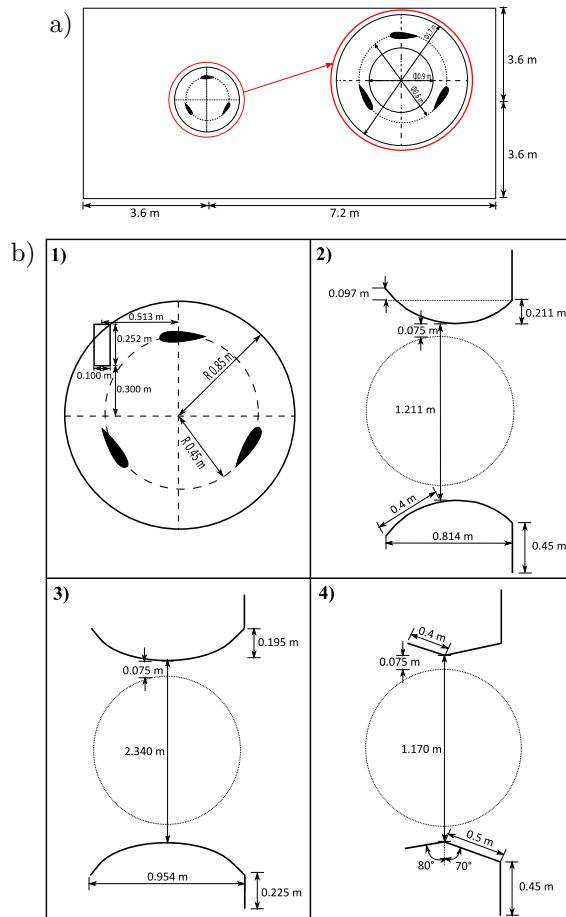

FIG. 1. General dimensions of the configured models (own source): a) background grid dimensions for the baseline case, b) rotor dimensions and passive mechanisms: 1) rotor and blocking plate, 2) curve, 3) cycloidal, 4) flat plate.

2.3. Discretization and numerical method

Once the design of the rotors was completed, the discretization was performed in the ICEM CFD module of ANSYS® 2022. The turbine flow was considered turbulent to capture the inertial forces and viscous forces responsible for hydraulic losses [28]. Inflation was only applied to the blade walls, as these are the components of the system where the highest velocities occur.

Figure 2a shows the rotor meshes configured as a rotating domain. Figure 2b shows the blade discretization with mesh transformation applied for each blade position. Additionally, the blades are configured as a rotating domain due to their relative motion with the rotor. It is possible to identify the inflation performed on the blade walls, with a growth rate of 1.2. Moreover, Fig. 2c illustrates standard background grid, which corresponds to the stationary domain of the model, with refinement in the part where the rotating domain is located. Figure 2d shows all overlapping meshes in the baseline case. The mesh metrics are compiled in Table 1, and fall within the acceptable ranges as recommended by the ANSYS user manuals [29].
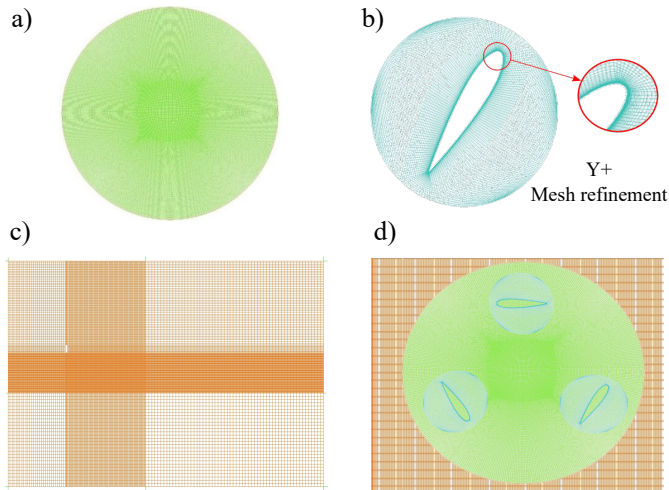

FIG. 2. Discretization of control surfaces (own source): a) rotor mesh, b) blade mesh, c) baseline background mesh, d) assembly by overlapping method.

To achieve mesh independence, five meshes with elements between 88E3 to 163E5 were used, the convergence criterion selected was efficiency, and the baseline case, with a solidity of 1.79 and a TSR of 1.5, was selected to carry out the mesh independence study.

The simulation is carried out using the commercial simulation tool Fluent from ANSYS® 2022. Boundary conditions are configured as shown in Fig. 3. An inlet velocity of 1 m/s is configured, with atmospheric pressure at the outlet.

Table 1. Mesh details and metrics (own source).

Components	Number of elements	Min. determinant $2 \times 2 \times 2$	Max. aspect ratio
Blade σ 1.79	8990	0.995	56.30
Blade σ 1.35	16 558	0.485	96.00
Blade σ 1.0	15 484	0.31	91.00
Rotor	57 321	0.948	3.07
Baseline	57 882	1.000	2.18
Curve	26 658	0.931	21.40
Cycloidal	23 615	0.883	10.40
Flat plate	16 539	0.981	42.70
Blocking plate	47 690	1.000	2.08
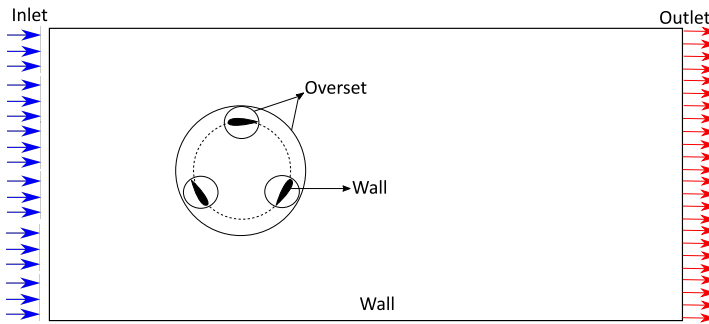
Fig. 3. Baseline model boundary conditions (own source).

On the other hand, the blade walls of the blades and the channel walls are set without slip to represent the rotor surfaces. Since the meshes overlap, interfaces are shared through the "overset" method, which allows for better control over the behavior of each domain [30].

The total simulation time for all cases is 10 s with a time step of 0.005 s and 2000 iterations. The control variables are C_p and C_T, which display a harmonic behavior once the simulation is stabilized. Table 2 summarizes the conditions configured in the simulations.

Table 2. Boundary conditions employed in the present study (own source).

Parameter	Value
Type of simulation	Transient
Turbulence model	$k - \varepsilon$ realizable
Angular velocity	2.22 to 10 rad/s
Temperature	25°C
Pressure	1 atm

In the present study, the $k - \varepsilon$ realizable turbulence model was used because of its correct prediction of turbine behavior and its reasonable computational cost in comparison to other turbulence models available in the solver [28, 31–34]. The transport equations for k and ε in this turbulence model are given by the following equations [35]:

$$(2.8) \quad \frac{\partial}{\partial t}(\rho k) + \frac{\partial}{\partial x_i}(\rho k U_j) = \frac{\partial}{\partial x_i}\left[\left(\mu + \frac{\mu_t}{\sigma_k}\right)\frac{\partial \kappa}{\partial x_j}\right] + G_k + G_b - \rho \varepsilon - Y_M + S_k,$$

$$(2.9) \quad \frac{\partial}{\partial t}(\rho \varepsilon) + \frac{\partial}{\partial x_j}(\rho \varepsilon U_j) = \frac{\partial}{\partial x_j}\left[\left(\mu + \frac{\mu_t}{\sigma_\varepsilon}\right)\frac{\partial \varepsilon}{\partial x_j}\right] + \rho C_1 S_t$$

$$- \rho C_2 \frac{\varepsilon^2}{k + \sqrt{v\varepsilon}} + C_{1\varepsilon}\frac{\varepsilon^2}{\kappa}C_{3\varepsilon}G_b + S_t,$$

where

$$(2.10) \qquad\qquad C_1 = \max\left[0.43\frac{\eta}{\eta + 5}\right],$$

$$(2.11) \qquad\qquad \eta = S\frac{k}{\varepsilon},$$

$$(2.12) \qquad\qquad S = \sqrt{2S_{ij}S_{ij}},$$

where G_k is the generation of turbulence kinetic energy caused by velocity gradients, G_b is the generation of turbulence kinetic energy due to buoyancy. Furthermore, Y_M is the contribution of fluctuating diffusion in compressible turbulence to the overall dissipation rate, σ_k and σ_ε are the turbulent Prandtl numbers for k and ε, respectively, and S_k and S_ε are user-defined source terms.

3. Results and discussion

Various parameters can be evaluated in the performance of HDTs. However, this work focuses on examining the behavior of the net moment coefficient for each configured turbine and the development of the power coefficient at various TSRs.

Figure 4 represents the mesh independence study carried out with the baseline case with a TSR of 1.5. The mesh selection criterion used is that the difference in results must be less than 5% with respect to the previous mesh, thus ensuring that the number of elements does not affect the results [36, 37]. The selected mesh contains 133E3 elements, with a difference of less than 2% compared the following meshes.
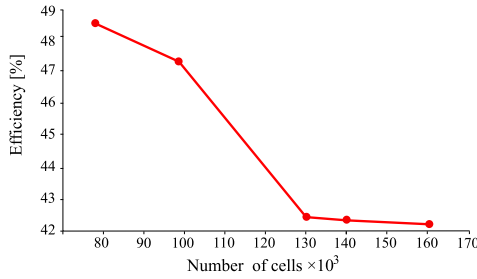
Fig. 4. Mesh independence study (own source).

3.1. Effect of accessories on C_t

Figure 5 shows the variation of the total C_t in one revolution for each of the configured cases (solidities of 1.0, 1.35, and 1.79) at a TSR of 2.5. A dotted line indicating zero, helps marking when the C_t is positive or negative. Figure 5a shows that the baseline σ 1.0 case exhibits an atypical behavior compared to the other baseline cases. Conversely, the other configurations demonstrate oscillations along the positive and negative y-axis (except for the cycloidal case). In Fig. 5b, the cases exhibit a stable behavior and remain mostly in the entire area of the curve in the positive y-axis. In Fig. 5c, the cycloidal and curve cases show large fluctuations, while the other cases exhibit greater stability along the complete turn. It is evident that these cases display more irregularities in behavior of the different cases with respect to their counterparts with different solidities. In general, the best performing cases are the configurations with flat plate and curve, which always remain in the positive y-axis.

By examining the behavior of the total C_t in the simulations, it is possible to eliminate some passive mechanisms for low efficiency. In Fig. 6, cases with better performance are observed. These cases have their operating areas in the positive y-axis, which indicates that the net power is positive. The maximum C_t is achieved by the flat plate case, with solidities of 1.79 and 1.35, respectively.

Table 3 shows the results obtained numerically for each of the cases proposed at a TSR of 2.5, including the average C_t and C_p. It is evident that the cases with the best efficiencies also correspond to the best C_t. When C_t is negative, the net power is also negative, which translates into inefficiency. This also indicates that these passive mechanisms are not useful, although most of them present higher efficiency percentages concerning the baseline case. The best case is the flat plate configuration with an efficiency of approximately 118%, and the increased factor for the baseline case equal to 7.713. The improvement by implementing passive mechanisms is remarkable, and this is consistent with that reported by HASHEM et al. [23], where an increase of C_p from 0.34 to 1.36 was achieved for an HDT configured with an external accessory. However, it should be noted that,
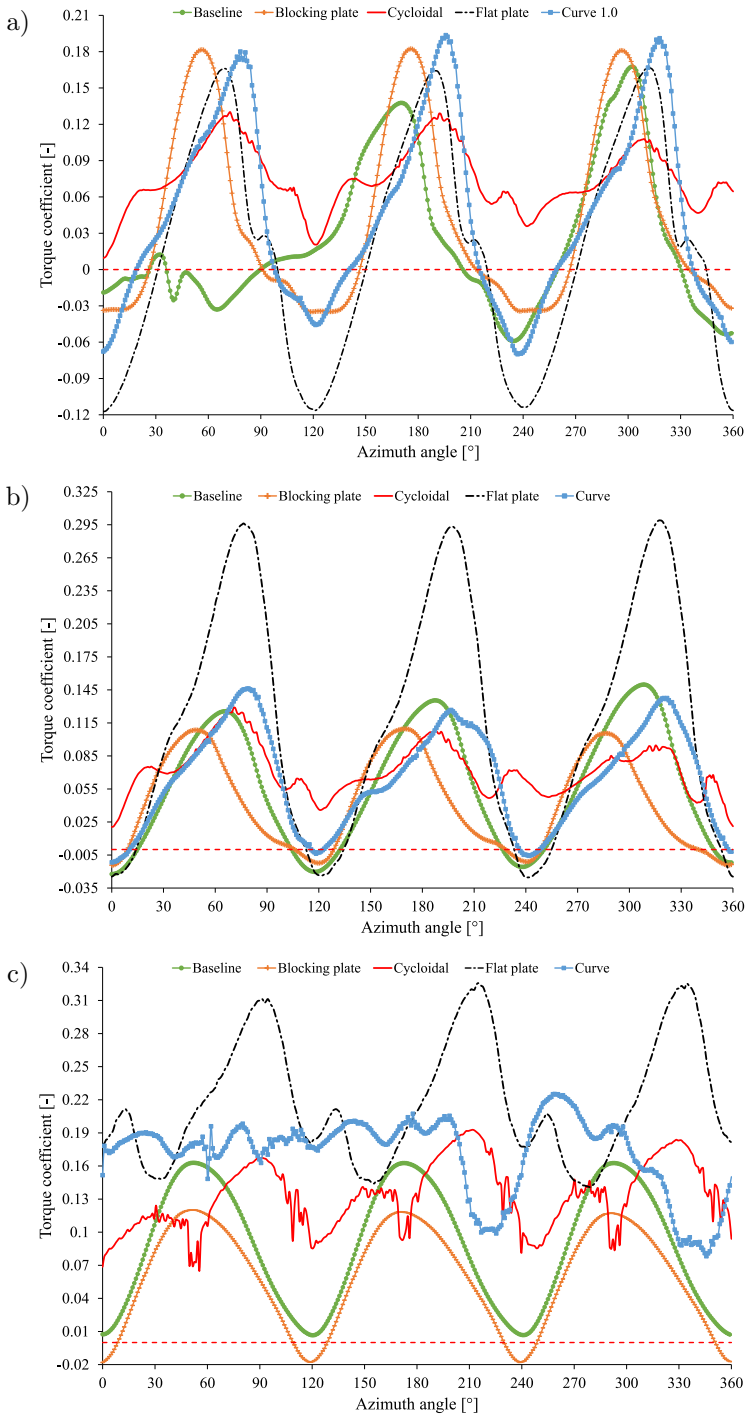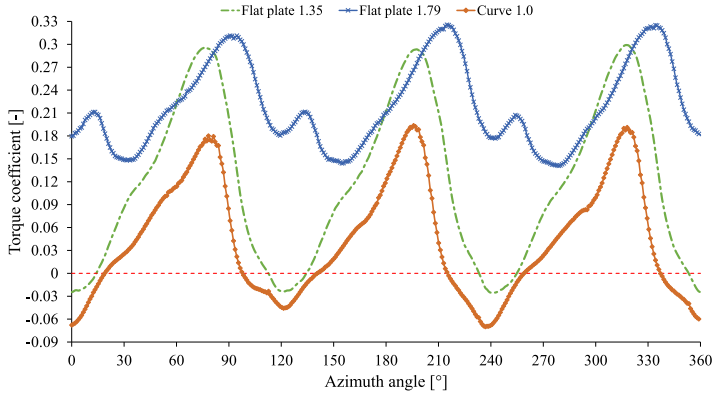
FIG. 5. Variation of total C_t in all cases (own source):
a) solidity 1.0, b) solidity 1.35, c) solidity 1.79.

FIG. 6. Best variation of total C_t (own source).

Table 3. Comparison of numerical results. TSR 2.5 (own source).

Solidity [-]	Configuration	C_m [-]	Average torque [N·m]	Power [W]	C_p [-]	Efficiency [%]
1.0	Baseline	0.0179	10.967	60.869	0.136	13.567
	Flat plate	0.1337	81.888	454.481	1.013	101.300
	Curve	0.1352	82.825	459.676	1.025	102.458
1.35	Baseline	0.020	12.349	68.611	0.153	15.293
	Flat plate	0.156	95.254	529.230	1.180	117.960
	Curve	0.110	67.469	374.856	0.836	83.552
1.79	Baseline	0.007	4.358	24.215	0.054	5.397
	Flat plate	0.139	85.179	473.253	1.055	105.484
	Curve	0.078	47.784	265.489	0.592	59.175

although the design of the accessories was emulated, in their study the authors changed parameters such as profiles and inlet velocity, and the working fluid was air. Similarly, PATEL *et al.* [38] implemented a blocking plate on the periphery of an H-Darrieus hydrokinetic turbine obtaining an increase in C_p from 0.125 to 0.35 with a rotor diameter of 0.265 m.

3.2. Effect of accessories on C_p

The behavior of the power coefficient C_p versus TSR is typically a parabolic curve, indicating a range of TSR where maximum efficiency is achieved. According to MOHAMED *et al.* [18], increasing the solidity results in the maximum C_p obtained at lower TSR. This behavior is illustrated in Fig. 7 where C_p versus TSR for all cases is observed. The flat plate and curve cases present the maximum C_p, because these passive mechanisms are more intrusive and increase mass flow and fluid velocity. Increasing the velocity, the rotor may extract more kinetic energy from the system, improving the efficiency. The implementation of
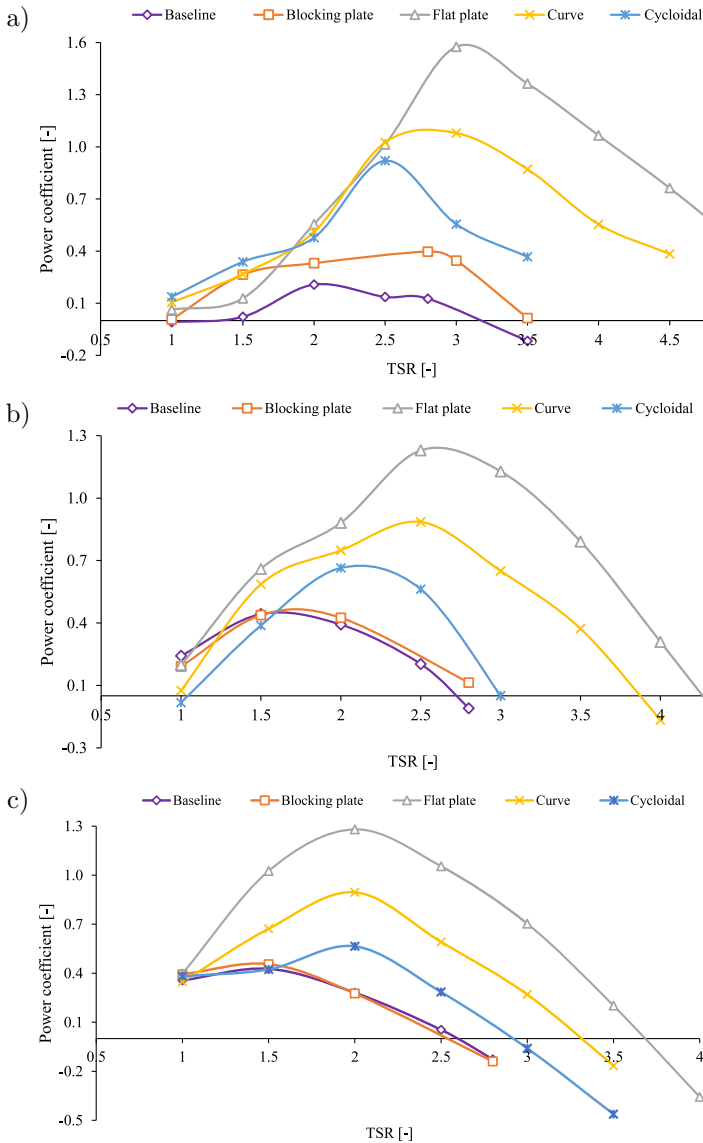
FIG. 7. Performance of all cases at different TSRs (own source):
a) solidity 1.0, b) solidity 1.35, c) solidity 1.79.

the passive mechanisms produces maximum C_p that exceeds the Betz limit. This is because these mechanisms cause the mass flow to increase, which accelerates the fluid inside the turbine and decreases the pressure [39–41].

Table 4 shows the maximum C_p for all the configurations evaluated numerically. It clearly demonstrates the improvement of H-Darrieus hydrokinetic turbines when configured with passive mechanisms. For all solidities, the flat

Table 4. Best C_p in all cases (own source).

Configuration solidity 1.0	$C_{p,\max}$ [–]	Configuration solidity 1.35	$C_{p,\max}$ [–]	Configuration solidity 1.79	$C_{p,\max}$ [–]
Baseline	0.207	Baseline	0.392	Baseline	0.427
Curve	1.079	Curve	0.835	Curve	0.895
Cycloidal	0.920	Cycloidal	0.614	Cycloidal	0.565
Flat plate	1.576	Flat plate	1.180	Flat plate	1.280
Blocking plate	0.397	Blocking plate	0.387	Blocking plate	0.456

plate and curve passive mechanisms achieved the best performance, with an improvement of 660% and 420%, respectively, compared to the baseline σ 1.0 case. However, the baseline σ 1.0 case obtained the worst performance, in comparison to the other cases. In most cases, there is no linear behavior in the improvement of C_p with increasing or decreasing solidity.

The present study surpasses the power augmentation factor (PAF) reported by HASHEM *et al.* [23] with a maximum PAF of 3.9 for an HDT configured with a Venturi-shaped attachment as one of the cases studied in this research (flat plate case). These differences in PAF can be attributed to variations in inlet conditions, type of fluid, and blade profile implemented in their study, which differ from the simulations carried out in this study.

Figure 8 shows the velocity contour of the flat plate case with the TSR where the highest efficiency was achieved. When the solidity is 1.0, the velocities de-
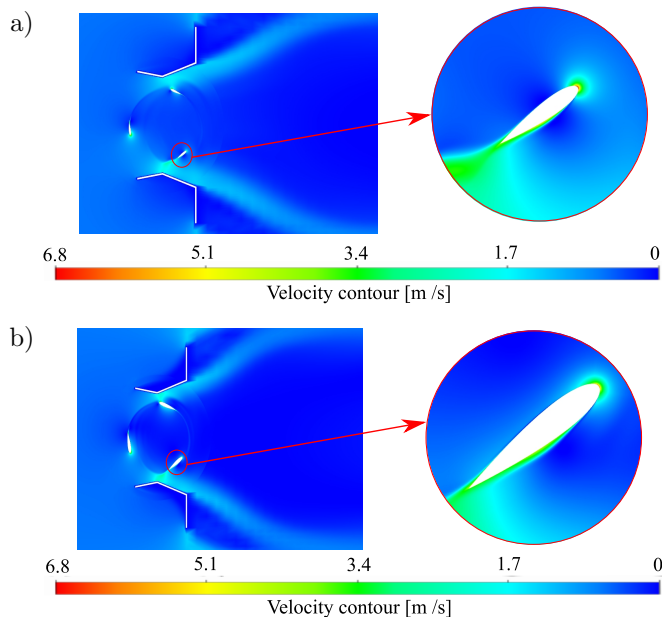
FIG. 8. Velocity flat plate cases (own source): a) solidity 1.0, 3.0 TSR, b) solidity 1.79, 2.0 TSR.

veloped inside are higher compared to those developed when the solidity is 1.79. This is particularly evident in the internal wake of the blades where the magnitude of velocity differs. The lower the solidity, the easier it is to extract kinetic energy from the system.

4. Concluding remarks

A numerical comparison was conducted for five H-Darrieus rotors with a symmetric NACA 0018 profile and solidities of 1.0, 1.35, and 1.79, each configured with four passive mechanisms located at the rotor's periphery. This study was carried out using ANSYS Fluent® 2022R1. The results can be summarized as follows:

- The performance of the H-Darrieus rotor improves by implementing passive mechanisms. The presence of these passive mechanisms affects both the power and the TSR.
- The H-Darrieus rotor configuration with passive mechanisms in diffuser geometry improves the self-starting capability due to increased positive torque.
- Among the four passive mechanisms implemented, the flat plate case with solidity of 1.0 presented the best performance, with a percentage improvement of 660% concerning the baseline σ 1.0 case.
- For future work, it is necessary to carry out the experimental validation of the different models proposed, especially for the baseline case and the flat plate case.

References

1. IEA, *Global Energy Review 2020*, Paris, 2020, https://www.iea.org/reports/global-energy-review-2020/renewables#abstract (accessed: Jan. 26, 2022).

2. Balkhair K.S., Rahman K.U., Sustainable and economical small-scale and low-head hydropower generation: A promising alternative potential solution for energy generation

at local and regional scale, *Applied Energy*, **188**: 378–391, 2017, doi: 10.1016/j.apenergy.2016.12.012.

3. Khan M.J., Bhuyan G., Iqbal M.T., Quaicoe J.E., Hydrokinetic energy conversion systems and assessment of horizontal and vertical axis turbines for river and tidal applications: A technology status review, *Applied Energy*, **86**(10): 1823–1835, 2009, doi: 10.1016/j.apenergy.2009.02.017.

4. Anyi M., Kirke B., Tests on a non-clogging hydrokinetic turbine, *Energy for Sustainable Development*, **25**: 50–55, 2015, doi: 10.1016/j.esd.2015.01.001.

5. Yuce M.I., Muratoglu A., Hydrokinetic energy conversion systems: A technology status review, *Renewable and Sustainable Energy Reviews*, **43**: 72–82, 2015, doi: 10.1016/j.rser.2014.10.037.

6. Aristizábal-Tique V.H., Villegas-Quiceno A.P., Arbeláez-Pérez O.F., Colmenares-Quintero R.F., Vélez-Hoyos F.J., Development of riverine hydrokinetic energy systems in Colombia and other world regions: A review of case studies, *DYNA*, **88**(217): 256–264, 2021, doi: 10.15446/dyna.v88n217.93098.

7. Khan M.J., Iqbal M.T., Quaicoe J.E., River current energy conversion systems: Progress, prospects and challenges, *Renewable and Sustainable Energy Reviews*, **12**(8): 2177–2193, 2008, doi: 10.1016/j.rser.2007.04.016.

8. Sornes K., *Small-scale Water Current Turbines for River Applications*, 2010, www.zero.no (accessed: Apr. 03, 2020).

9. Guney M.S., Evaluation and measures to increase performance coefficient of hydrokinetic turbines, *Renewable and Sustainable Energy Reviews*, **15**(8): 3669–3675, 2011, doi: 10.1016/j.rser.2011.07.009.

10. Mon E.E., Design of low head hydrokinetic turbine, *International Journal of Trend in Scientific Research and Development (IJTSRD)*, **3**(5): 2106–2109, 2019, https://www.ijtsrd.com/papers/ijtsrd27865.pdf.

11. Bel Mabrouk I., El Hami A., Effect of number of blades on the dynamic behavior of a Darrieus turbine geared transmission system, *Mechanical Systems and Signal Processing*, **121**: 562–578, 2019, doi: 10.1016/j.ymssp.2018.11.048.

12. Castelli M.R., Betta S. De, Benini E., Effect of blade number on a straight-bladed vertical-axis Darreius wind turbine, *World Academy of Science, Engineering and Technology, International Journal of Aerospace and Mechanical Engineering,* **6**(1): 256–262, 2012, doi: 10.5281/zenodo.1079974.

13. Hameed M.S., Afaq S.K., Design and analysis of a straight bladed vertical axis wind turbine blade using analytical and numerical techniques, *Ocean Engineering*, **57**: 248–255, 2013, doi: 10.1016/j.oceaneng.2012.09.007.

14. Rezaeiha A., Montazeri H., Blocken B., Towards optimal aerodynamic design of vertical axis wind turbines: Impact of solidity and number of blades, *Energy*, **165** (Part B): 1129–1148, 2018, doi: 10.1016/j.energy.2018.09.192.

15. Ahmadi-Baloutaki M., Carriveau R., Ting D.S.K., Straight-bladed vertical axis wind turbine rotor design guide based on aerodynamic performance and loading analysis, *Proceedings of the Institution of Mechanical Engineers, Part A: Journal of Power and Energy*, **228**(7): 742–759, 2014, doi: 10.1177/0957650914538631.

16. Tobon-Tobon N., Henao-González K.A., Burbano-Hernandez A.F., Sierra-Del Rio J., Hincapié Zuluaga D.A., Influence of the solidity and the number of blades in a vertical axis turbine type H-Darrieus [in Spanish: Influencia de la solidez y el número de

álabes en una turbina de eje vertical tipo h-darrieus], Revista Politécnica, **16**(32): 9–18, 2020, doi: 10.33571/rpolitec.v16n32a1.

17. DU L., INGRAM G., DOMINY R.G., Experimental study of the effects of turbine solidity, blade profile, pitch angle, surface roughness, and aspect ratio on the H-Darrieus wind turbine self-starting and overall performance, *Energy Science and Engineering*, **7**(6): 2421–2436, 2019, doi: 10.1002/ese3.430.

18. MOHAMED M.H., Impacts of solidity and hybrid system in small wind turbines performance, *Energy*, **57**: 495–504, 2013, doi: 10.1016/j.energy.2013.06.004.

19. GUEVARA-MUNOZ A., HINCAPIE-ZULUAGA D., SIERRA-DEL RIO J., RODRIGUEZ-CA-BAL M.A., TORRES-LOPEZ E., Numerical comparison and efficiency analysis of three vertical axis turbine of H-Darrieus type, *EUREKA: Physics and Engineering*, **2**: 28–39, 2023, doi: 10.21303/2461-4262.2023.002593.

20. GOSSELIN R., DUMAS G., BOUDREAU M., Parametric study of H-Darrieus vertical-axis turbines using CFD simulations, *Journal of Renewable and Sustainable Energy*, **8**(5): 053301, 2016, doi: 10.1063/1.4963240.

21. KUMAR P.M., AJIT K.R., SURYA M.R., SRIKANTH N., LIM T.C., On the self starting of Darrieus turbine: An experimental investigation with secondary rotor, *Asian Conference on Energy, Power and Transportation Electrification*, **2017**: 1–7, 2017, doi: 10.1109/ACEPT.2017.8168545.

22. SHIMOKAWA K., FURUKAWA A., OKUMA K., MATSUSHITA D., WATANABE S., Experimental study on simplification of Darrieus-type hydro turbine with inlet nozzle for extra-low head hydropower utilization, *Renewable Energy*, **41**: 376–382, 2012, doi: 10.1016/j.renene.2011.09.017.

23. HASHEM I., MOHAMED M.H., Aerodynamic performance enhancements of H-rotor Darrieus wind turbine, *Energy*, **142**: 531–545, 2018, doi: 10.1016/j.energy.2017.10.036.

24. TUNIO I.A., SHAH M.A., HUSSAIN T., HARIJAN K., MIRJAT N.H., MEMON A.H., Investigation of duct augmented system effect on the overall performance of straight blade Darrieus hydrokinetic turbine, *Renewable Energy*, **153**: 143–154, 2020, doi: 10.1016/j.renene.2020.02.012.

25. PATEL V., ELDHO T.I., PRABHU S.V., Performance enhancement of a Darrieus hydrokinetic turbine with the blocking of a specific flow region for optimum use of hydropower, *Renewable Energy*, **135**: 1144–1156, 2019, doi: 10.1016/j.renene.2018.12.074.

26. JANON A., Torque coefficient analysis of a novel direct-drive parallel-stream counter-rotating Darrieus turbine system, *Renewable Energy*, **147** (Part 1): 110–117, 2020, doi: 10.1016/j.renene.2019.08.118.

27. ALAM M.J., IQBAL M.T., Design and development of hybrid vertical axis turbine, *2009 Canadian Conference on Electrical and Computer Engineering*, **978**: 1178–1183, 2009, doi: 10.1109/CCECE.2009.5090311.

28. DARÓCZY L., JANIGA G., PETRASCH K., WEBNER M., THÉVENIN D., Comparative analysis of turbulence models for the aerodynamic simulation of H-Darrieus rotors, *Energy*, **90**(1): 680–690, 2015, doi: 10.1016/j.energy.2015.07.102.

29. Ansys Inc., *User Manual Ansys ICEM CFD 12.1*, 0844682: 724–746, 2009.

30. CARRICA P.M., WILSON R.V., NOACK R.W., STERN F., Ship motions using single-phase level set with dynamic overset grids, *Computers & Fluids*, **36**(9): 1415–1433, 2007, doi: 10.1016/J.COMPFLUID.2007.01.007.

31. WANG S., INGHAM D.B., MA L., POURKASHANIAN M., TAO Z., Turbulence modeling of deep dynamic stall at relatively low Reynolds number, *Journal of Fluids and Structures*, **33**: 191–209, 2012, doi: 10.1016/j.jfluidstructs.2012.04.011.

32. ALMOHAMMADI K.M., INGHAM D.B., MA L., POURKASHAN M., Computational fluid dynamics (CFD) mesh independency techniques for a straight blade vertical axis wind turbine, *Energy*, **58**: 483–493, 2013, doi: 10.1016/j.energy.2013.06.012.

33. LANZAFAME R., MAURO S., MESSINA M., 2D CFD modeling of H-Darrieus wind turbines using a transition turbulence model, *Energy Procedia*, **45**: 131–140, 2014, doi: 10.1016/j.egypro.2014.01.015.

34. MARSH P., RANMUTHUGALA D., PENESIS I., THOMAS G., The influence of turbulence model and two and three-dimensional domain selection on the simulated performance characteristics of vertical axis tidal turbines, *Renewable Energy*, **105**: 106–116, 2017, doi: 10.1016/j.renene.2016.11.063.

35. MOHAMED M.H., ALI A.M., HAFIZ A.A., CFD analysis for H-rotor Darrieus turbine as a low speed wind energy converter, *Engineering Science and Technology, an International Journal*, **18**(1): 1–13, 2015, doi: 10.1016/j.jestch.2014.08.002.

36. CASTAŃEDA-CEBALLOS L., CARDONA-VALENCIA M., HINCAPIÉ-ZULUAGA D., SIERRA-DEL RIO J., VÉLEZ-GARCIA S., Influence of the number of blades in the power generated by a Michell Banki turbine, *International Journal of Renewable Energy Research*, **7**(4): 1989–1997, 2017, doi: 10.20508/ijrer.v7i4.6372.g7246.

37. BELTRAN-URANGO D., HERRERA-DÍAZ J.L., POSADA-MONTOYA J.A., CASTAŃEDA L., SIERRA-DEL RIO J.A., Generation of electric power through gravitational vortices [in Spanish: Generación de Energía Eléctrica Mediante Vórtices Gravitacionales], *Memorias EXPO Tecnologias 2016*, Medellin, Antioquia, pp. 90–107, 2016.

38. PATEL V., ELDHO T.I., PRABHU S.V., Experimental investigations on Darrieus straight blade turbine for tidal current application and parametric optimization for hydro farm arrangement, *International Journal of Marine Energy*, **17**: 110–135, 2017, doi: 10.1016/j.ijome.2017.01.007.

39. HANSEN M.O.L., SŘRENSEN N.N., FLAY R.G.J., Effect of placing a diffuser around a wind turbine, *Wind Energy*, **3**(4): 207–213, 2000, doi: 10.1002/WE.37.

40. OHYA Y., KARASUDANI T., SAKURAI A., INOUE M., Development of a high-performance wind turbine equipped with a brimmed diffuser shroud, *Transactions of the Japan Society for Aeronautical and Space Sciences*, **49**(163): 18–24, 2006, doi: 10.2322/tjsass.49.18.

41. JAMIESON P.M., Beating Betz: Energy extraction limits in a constrained flow field, *Journal of Solar Energy Engineering, Transactions of the ASME*, **131**(3): 031008, 2009, doi: 10.1115/1.3139143.